Andrzej Zachara,
***Zbigniew Lewandowski**

Institute of Fundamental Technological Research, Polish Academy of Sciences, Warsaw
ul. Świętokrzyska 21, 00-049 Warszawa, Poland,
E-mail: azachara@ippt.gov.pl

***University of Bielsko-Biała,**
ul. Willowa 2, 43-309 Bielsko-Biała, Poland,
E-mail: z.lewandowski@wp.pl

Mathematical Modelling of Pneumatic Melt Spinning of Isotactic Polypropylene. Part I. Modelling of the Air Jet Dynamics

Abstract
In this series of publications, the process of nonwoven melt blowing of ultra-fine fibers is presented. The process starts in the dual slot die where two converging air jets draw the molten polymer stream. In the present paper (Part I), the air flow field is investigated with the aid of the k – ε turbulence model, which is solved numerically. From the results of computations, we have distributions of the air flow parameters along the z – axis, which is also the axis of pneumatic melt spinning. These parameters are the air velocity, temperature and pressure, which will be used in Part II and III to compute the fiber melt blowing dynamics.

Key words: *fiber spinning, melt blowing, nonwoven, computational fluid dynamics, turbulence model.*

Introduction

Pneumatic melt spinning provides an alternative technique for obtaining non-woven mats of ultra-fine fibers with a high surface-to-mass ratio, which is important for biomedical, biotechnological and filtration, applications, among others. The pneumatic process consists in the uniaxial drawing of a molten polymer stream by two converging air jets directed symmetrically on both sides of a two-slot die [1, 2]. The polymer stream attenuates rapidly just below the spinneret face, under intensive uniaxial deformation caused by a pneumatic tensile force which results from the transfer of momentum between the air jets and polymer melt along the spinning axis. The process is accompanied by heat exchange between the jets and polymer stream depending on the local temperature difference between this media along the spinning line. One can expect that the solidification of the spun filament which occurs by glass transition or crystallisation, and the diameter of the fibers obtained in the non-woven are affected by the initial temperature and velocity of the air jets, as well as by the distribution of the air temperature and velocity along the spinning axis. With the application of standard polymers, such as polypropylene, polyethylene, polyesters, polyamides, as well as elastomers and polymers of biotechnological importance, the thickness of fibers in the pneumatic spun non-wovens is reported to be in the range of 1 - 5 μm in the case of fine fibers obtained in the process [3 - 5].

It is important to determine the conditions for the stationary process of pneumatic melt spinning necessary for obtaining regular non-woven with uniform fibers, as well as to learn the role of various processing conditions regarding the thickness and structure of the fibers, which is important from the point of view of the nonwoven properties. Mathematical modelling and computer simulation open the possibility of low cost investigations on pneumatic melt spinning, which are expected to provide information on the character of individual processing and material parameters necessary for optimising the process of obtaining non-woven of desirably fine fibers with favorable structure. The modeling akso allows to investigate the dynamics of the process along the spinning axis between the melt outflow from the spinneret orifice and the take-up point on the surface of the nonwoven, and to determine axial profiles of the velocity, temperature, tensile stress, hydrostatic pressure, molecular orientation and crystallinity of the polymer.

In the pneumatic process the double air jet constitutes a medium transferring momentum to the polymer stream and exchanging the heat energy. The distributions of the air velocity and temperature along the spinning line play crucial role in the dynamics of the process and thickness of the fibers obtained. In this paper, being Part I of a series on pneumatic melt spinning, the fundamentals of the modelling of the air velocity, temperature and pressure fields in the air jet, necessary for discussing the dynamics of the pneumatic process, are presented. A mathematical model of pneumatic melt spinning with predetermined velocity, temperature and pressure of the air along the spinning axis, together with example computations performed for isotactic polypropylene will be presented in Parts II and III of the series of publications.

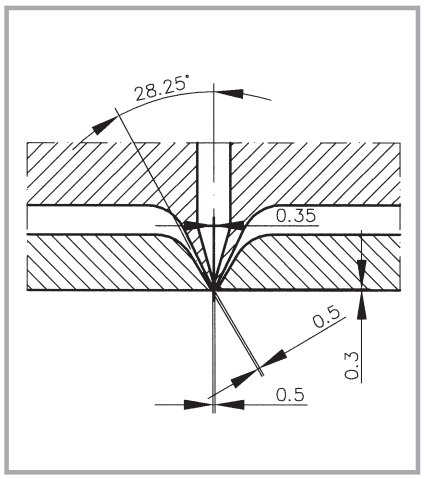

Figure 1. *Dual slot die geometry of the spinning beam in the (y,z) plane. The width of the slot die at the air outflow - 0.5 mm, the incline angle of the die slots to the z axis - 28.25º at the air output, diameter of the orifice in the spinneret - 0.35 mm, the distance between the air die slots at the spinneret level- 0.5 mm, the recession of the spinneret in the spinning beam – 0.3 mm.*

In this article we present a schematic view of a device where such pneumatic melt spinning is realized. A schematic diagram of a dual slot air die, a cross-section normal to the symmetry plane of the spinning beam, is shown in ***Figure 1***. In the diagram the polymer melt is extruded from the spinneret orifice and elongated by the air jet in the z-direction along the centerline. Two air jets are blown symmetrically from the left and right slots inclined to the z-axis at an angle α. The length of the air slots in the x-direction, vertical to the plane (y,z) in ***Figure 1***, is so large compared to its width at the outflow point that the air flow may be considered as two-dimensional in the y,z coordinate system. The experimental results show that the polymer melt which moves along the centerline z-axis is so narrow that its influence on the air flow dynamics may be neglected. Such a process was the subject of papers by Chen et al. [6], Krutka et al. [7] and [14]. In these papers the air flow was considered as turbulent and a compressible medium. The flow field was calculated numerically with the aid of the k – ε model in [6] and Reynolds stress model in [14]. In our paper the air flow field is calculated using the standard k - ε model of turbulent flow, in which the air is treated as a compressible fluid, including, as a consequence, the second viscosity coefficient ζ in the viscous stress tensor. The results of the computations will be used in Parts II and III of the publication, where the factors of fiber melt blowing will be calculated.

k - ε model of the turbulent flow

A mathematical model of turbulent flow, known in the literature as the *k* - ε model, will be used to determine the velocity, temperature, and pressure fields of double air jets, which are necessary to define the dynamic conditions of pneumatic melt spinning, with *k* being the turbulent kinetic energy of the air and ε its dissipation rate [8 - 10]. The model consists of a system of six partial differential equations for the mass continuity, momentum conservation in the (*y,z*) plane, energy conservation, turbulent kinetic energy and the turbulent dissipation rate. Constitutive fluid equations are also needed for the model presented.

The mass continuity and momentum conservation equations in their general form read as such

$$\frac{\partial}{\partial x_i}(\rho U_i) = 0 \tag{1}$$

$$\rho U_j \frac{\partial U_i}{\partial x_j} = -\frac{\partial P}{\partial x_i} + \frac{\partial}{\partial x_j}(t_{ij} - \tau_{ij}) + F_i \tag{2}$$

where ρ is the local air density, U_i - components of the air velocity vector, P - the air pressure, t_{ij} - viscous stress tensor components, τ_{ij} - Reynolds stress tensor components, and F_i - components of the buoyant force vector. They all are mean values of the turbulent quantities. We use Einstein's summation convention in the formulae.

The air in the model is treated as a compressible fluid. Hence, according to the theory of viscous and compressible Newtonian fluid [10], the viscous stress tensor t_{ij} is controlled by two viscosity coefficients, μ and ς

$$t_{ij} = \mu\left(\frac{\partial U_i}{\partial x_j} + \frac{\partial U_j}{\partial x_i}\right) + \varsigma \frac{\partial U_k}{\partial x_k}\delta_{ij} \tag{3}$$

It is widely accepted in the literature that the second viscosity coefficient is $\zeta = -2\mu/3$ and then the viscous stress tensor assumes the form

$$t_{ij} = \mu\left(\frac{\partial U_i}{\partial x_j} + \frac{\partial U_j}{\partial x_i} - \frac{2}{3}\frac{\partial U_k}{\partial x_k}\delta_{ij}\right) \tag{4}$$

For incompressible fluid the last term in the above expression vanishes.

Reynolds stress tensor is expressed by the relation [8, 10]

$$\begin{aligned}\tau_{ij} &= -\left\langle \rho u_i u_j \right\rangle = \\ &= \rho \nu_T \left(\frac{\partial U_i}{\partial x_j} + \frac{\partial U_j}{\partial x_i} - \frac{2}{3}\frac{\partial U_k}{\partial x_k}\delta_{ij}\right) - \frac{2}{3}\rho k \delta_{ij}\end{aligned} \tag{5}$$

where u_i are components of the fluctuating air velocity vector; $\langle\cdot\rangle$ denotes the average of the fluctuating velocity. The turbulent kinematic viscosity coefficient ν_T is determined from the relation [6, 9, 11]

$$\nu_T = C_\mu \frac{k^2}{\varepsilon} \tag{6}$$

where C_μ is a constant, k - the turbulent kinetic energy, and ε - the dissipation rate of the turbulent energy.

The buoyant force F_i in Equation (2), which acts in a vertical *z*–direction, may be expressed as

$$F_i = (\rho_\infty - \rho) g \tag{7}$$

where ρ_∞ is the air density in ambient conditions, and g – the gravity acceleration.

$$\rho U_y \frac{\partial U_y}{\partial y} + \rho U_z \frac{\partial U_y}{\partial z} = -\frac{\partial P}{\partial y} + \frac{2}{3}\frac{\partial}{\partial y}\left[\rho(\nu + \nu_T)\left(2\frac{\partial U_y}{\partial y} - \frac{\partial U_z}{\partial z}\right) - \rho k\right] + \frac{\partial}{\partial z}\left[\rho(\nu + \nu_T)\left(\frac{\partial U_y}{\partial z} + \frac{\partial U_z}{\partial y}\right)\right] \tag{10}$$

$$\rho U_y \frac{\partial U_z}{\partial y} + \rho U_z \frac{\partial U_z}{\partial z} = -\frac{\partial P}{\partial z} + \frac{\partial}{\partial y}\left[\rho(\nu + \nu_T)\left(\frac{\partial U_z}{\partial y} + \frac{\partial U_y}{\partial z}\right)\right] + \frac{2}{3}\frac{\partial}{\partial z}\left[\rho(\nu + \nu_T)\left(2\frac{\partial U_z}{\partial z} - \frac{\partial U_y}{\partial y}\right) - \rho k\right] + \rho g\left(\frac{T}{T_\infty} - 1\right) \tag{11}$$

where $\nu = \mu/\rho$ is the kinematic viscosity.

$$\frac{\partial}{\partial x_j}\left[U_j(\rho E + P)\right] = \frac{\partial}{\partial x_j}\left[(\lambda + \lambda_T)\frac{\partial T}{\partial x_j}\right] + \frac{\partial}{\partial x_j}\left[U_i(\tau_{ij})_{eff}\right] \tag{12}$$

Equations 10, 11, and 12.

From the law of thermal expansion, we get the following relation

$$\frac{1}{\rho}=\frac{1}{\rho_\infty}\left[1+\beta\left(T-T_\infty\right)\right] \tag{8}$$

where T is the absolute air temperature, T_∞ is the ambient air temperature, and $\beta = 1/T_\infty$ - the coefficient of the thermal volume expansion. Equations (7) and (8) lead to the following formula for the z-component of the buoyant force vector

$$F_z=\rho g\left(\frac{T}{T_\infty}-1\right) \tag{9}$$

Thus momentum conservation equation (2) together with relations (4), (5) and (9) assume the form of the Cartesian coordinate system presented by Equations (10 and 11).

The energy conservation equation for the k - ε turbulent flow model is presented by Equation (12), where λ is the thermal conductivity coefficient, and λ_T – the thermal conductivity coefficient in the turbulent flow, which may be expressed by the Equation (13)

$$\lambda_T=\frac{C_p\rho\nu_T}{\sigma_T} \tag{13}$$

where C_p is the specific heat at constant pressure, σ_T - the turbulent Prandtl number, E - the total energy of the flowing air per unit mass, which is the sum of the internal energy, $E_w = C_vT$, and kinetic energy of the two-dimensional flow in the (y, z) plane, $E_k = V^2/2 = (U_y^2 + U_z^2)/2$. Hence, the total energy per unit mass of the air is

$$E=C_vT+\frac{V^2}{2} \tag{14}$$

where C_v is the specific heat at constant volume.

With relations (13) and (14), the energy conservation Equation (12) assumes the form (Equation 15).

In momentum conservation Equations (10) and (11), as well as in the energy conservation Equation (15), we deal with the turbulent viscosity coefficient ν_T and turbulent kinetic energy k. In the k - ε model of turbulence, the viscosity coefficient ν_T is determined by relation (6); after which we deal with the following two variables: the kinetic energy of turbulent motion

$$k=\frac{1}{2}\left\langle u_iu_i\right\rangle \tag{16}$$

and the dissipation rate of the turbulent kinetic energy

$$\varepsilon=\nu\left\langle\frac{\partial u_i}{\partial x_j}\cdot\frac{\partial u_j}{\partial x_i}\right\rangle \tag{17}$$

The kinetic energy k and dissipation rate ε are calculated from additional equations in the model. The turbulence kinetic energy equation [10] is given by (18) where p denotes the fluctuating air pressure, f_i - components of the fluctuating buoyant force.

The terms of the above equation have the following meaning: on the left hand side we have the energy of convection, and on the right side we have the following (one after the other): the turbulent energy production, the kinetic energy dissipation, the molecular diffusion with the turbulent transport of the turbulence kinetic energy, the pressure work, pressure dilatation, and the transport by the buoyant force fluctuation.

We have unknown quantities on the right hand side of Equation (18) which are correlations of the fluctuating parameters. To complete the system of equations, these quantities should be expressed by the known variables. For this reason we take into account the argumentation given in [10] and [11], where the authors suggest the approximation shown in Equation (19) for the terms where σ_K is the Prandtl number of the turbulent kinetic energy.

According to Wilcox [10], there is lack of information concerning diffusion by the pressure fluctuation, and the terms

$$-\left\langle u_i\frac{\partial p}{\partial x_i}\right\rangle \text{ and } -\left\langle p\frac{\partial u_i}{\partial x_i}\right\rangle$$

are usually neglected in mathematical modelling of the turbulent flow.

The last term in Equation (18), which presents energy transport by the buoyant force fluctuations, will be modelled using the following relation applied by Chen at al. [6] presented by Equation (20).

$$\left\langle f_iu_i\right\rangle=\rho g\frac{\nu_T}{\sigma_TT_\infty}\frac{\partial T}{\partial z} \tag{20}$$

Taking into account Equations (19), (20) and neglecting the work pressure and pressure dilatation terms, Equation (18) reduces to Equation (21).

$$\begin{aligned}&\rho U_y\frac{\partial}{\partial y}\left(C_vT+\frac{V^2}{2}+\frac{P}{\rho}\right)+\rho U_z\frac{\partial}{\partial z}\left(C_vT+\frac{V^2}{2}+\frac{P}{\rho}\right)+P\left(\frac{\partial U_y}{\partial y}+\frac{\partial U_z}{\partial z}\right)=\\&+\frac{\partial}{\partial y}\left(\lambda_{eff}\frac{\partial T}{\partial y}\right)+\frac{\partial}{\partial z}\left(\lambda_{eff}\frac{\partial T}{\partial z}\right)+\frac{2}{3}\frac{\partial}{\partial y}\left[\rho\nu_{eff}U_y\left(2\frac{\partial U_y}{\partial y}-\frac{\partial U_z}{\partial z}\right)-\rho k\right]+\\&+\frac{\partial}{\partial z}\left[\rho\nu_{eff}U_y\left(\frac{\partial U_z}{\partial y}+\frac{\partial U_y}{\partial z}\right)\right]+\frac{\partial}{\partial y}\left[\rho\nu_{eff}U_z\left(\frac{\partial U_z}{\partial y}+\frac{\partial U_y}{\partial z}\right)\right]+\\&+\frac{2}{3}\frac{\partial}{\partial z}\left[\rho\nu_{eff}U_y\left(2\frac{\partial U_z}{\partial z}-\frac{\partial U_y}{\partial y}\right)-\rho k\right]\end{aligned} \tag{15}$$

where $\nu_{eff} = \nu + \nu_T$ and $\lambda_{eff} = \lambda + \lambda_T$.

$$\begin{aligned}&\rho U_j\frac{\partial k}{\partial x_j}=\tau_{ij}\frac{\partial U_i}{\partial x_j}-\rho\varepsilon+\frac{\partial}{\partial x_j}\left[\left\langle t_{ij}u_i\right\rangle-\left\langle\rho u_j\frac{1}{2}u_iu_i\right\rangle-\left\langle pu_j\right\rangle\right]+\\&-\left\langle u_i\frac{\partial p}{\partial x_i}\right\rangle-\left\langle p\frac{\partial u_i}{\partial x_i}\right\rangle-\left\langle f_iu_i\right\rangle\end{aligned} \tag{18}$$

$$\left\langle t_{ij}u_i\right\rangle-\left\langle\rho u_j\frac{1}{2}u_iu_i\right\rangle-\left\langle pu_j\right\rangle=\rho\left(\nu+\frac{\nu_T}{\sigma_K}\right)\frac{\partial k}{\partial x_j} \tag{19}$$

$$\rho U_j\frac{\partial k}{\partial x_j}=\tau_{ij}\frac{\partial U_i}{\partial x_j}-\rho\varepsilon+\frac{\partial}{\partial x_j}\left[\rho\left(\nu+\frac{\nu_T}{\sigma_K}\right)\frac{\partial k}{\partial x_j}\right]-\rho g\frac{\nu_T}{\sigma_KT_\infty}\frac{\partial T}{\partial z} \tag{21}$$

$$\begin{aligned}&\rho\left[U_y\frac{\partial k}{\partial y}+U_z\frac{\partial k}{\partial z}\right]=P_K-\rho\varepsilon+\frac{\partial}{\partial y}\left[\rho\left(\nu+\frac{\nu_T}{\sigma_K}\right)\frac{\partial k}{\partial y}\right]+\frac{\partial}{\partial z}\left[\rho\left(\nu+\frac{\nu_T}{\sigma_K}\right)\frac{\partial k}{\partial z}\right]+\\&-\rho g\frac{\nu_T}{\sigma_KT_\infty}\frac{\partial T}{\partial z}\end{aligned} \tag{22}$$

Equations 15, 18, 19, 21, and 22.

Using the Cartesian coordinate system, we get Equation (22) where P_K is the turbulent energy production described by Equation (23), see page 20.

The expression for the kinetic energy dissipation rate, presented in [8], taking into account the influence of the buoyant force fluctuation, reads (24).

The left-hand side of the equation represents the convection of the dissipation rate. The consecutive terms on the right-hand side represent molecular, turbulent, and pressure diffusion, respectively, and the next three terms – extension of the spinning lines by the mean motion followed by the terms responsible for the turbulence generation by the spinning line deformation, destruction of the turbulence, and variation of the dissipation by the buoyancy force fluctuation. Taking into account an estimation of the terms in Equation (24), presented in [8], we neglect the term responsible for the effects of molecular diffusion, as well as three terms corresponding to the extension of the spinning lines by the mean motion. The sum of the turbulent and pressure diffusion terms is expressed by Equation (25) while the sum of the terms responsible for the turbulence generation by the spinning line deformation, and the destruction of turbulence may be presented as Equation (26) where σ_ε is the Prandtl number of the dissipation rate. The last term in Equation (24), which takes into account the influence of the buoyancy force fluctuation, may be presented as [6]

$$2\rho\nu\left\langle\frac{\partial f_i}{\partial x_k}\frac{\partial u_i}{\partial x_k}\right\rangle = C_{\varepsilon 1}\rho g\frac{\varepsilon}{k}\frac{\nu_T}{\sigma_T T_\infty}\frac{\partial T}{\partial z} \quad (27)$$

Hence, Equation (24) reduces to Equation (28).

Using the Cartesian coordinate system, we get Equation (29).

In the model presented we have eight unknown quantities: U_y , U_z – the velocity of the components in the y and z directions, ρ - the density, P – the pressure, T - the temperature, ν_T – the turbulent kinematic viscosity coefficient, k – the turbulent kinetic energy, and ε - the dissipation rate of the turbulent kinetic energy. These quantities will be calculated from the six

$$P_K = \tau_{ij}\frac{\partial U_i}{\partial x_j} = \frac{4}{3}\rho\nu_T\left[\left(\frac{\partial U_y}{\partial y}\right)^2 + \left(\frac{\partial U_z}{\partial z}\right)^2 - \frac{\partial U_y}{\partial y}\cdot\frac{\partial U_z}{\partial z}\right] + \quad (23)$$
$$+\rho\nu_T\left(\frac{\partial U_z}{\partial y} \quad \frac{\partial U_y}{\partial z}\right)^2 - \frac{2}{3}\rho k\left(\frac{\partial U_y}{\partial y} + \frac{\partial U_z}{\partial z}\right)$$

$$\rho U_j\frac{\partial\varepsilon}{\partial x_j} = -\frac{\partial}{\partial x_j}\left[-\rho\nu\frac{\partial\varepsilon}{\partial x_j} + \left\langle\rho\nu u_i\frac{\partial u_i}{\partial x_k}\cdot\frac{\partial u_j}{\partial x_k}\right\rangle + 2\nu\left\langle\frac{\partial u_j}{\partial x_k}\cdot\frac{\partial p}{\partial x_k}\right\rangle\right] +$$
$$-2\rho\nu\left[\left\langle\frac{\partial u_i}{\partial x_k}\cdot\frac{\partial u_j}{\partial x_k}\right\rangle\cdot\frac{\partial U_i}{\partial x_j} + \left\langle\frac{\partial u_i}{\partial x_k}\cdot\frac{\partial u_i}{\partial x_j}\right\rangle\cdot\frac{\partial U_j}{\partial x_k} + \left\langle u_j\frac{\partial u_i}{\partial x_k}\right\rangle\frac{\partial^2 U_i}{\partial x_k\partial x_j}\right] + \quad (24)$$
$$-2\rho\nu\left[\left\langle\frac{\partial u_i}{\partial x_k}\cdot\frac{\partial u_j}{\partial x_k}\cdot\frac{\partial u_i}{\partial x_j}\right\rangle + \nu\left\langle\frac{\partial^2 u_i}{\partial x_j\partial x_k}\right\rangle^2 + \left\langle\frac{\partial f_i}{\partial x_k}\frac{\partial u_i}{\partial x_k}\right\rangle\right]$$

$$-\frac{\partial}{\partial x_j}\left[\left\langle\rho\nu u_i\frac{\partial u_i}{\partial x_k}\cdot\frac{\partial u_j}{\partial x_k}\right\rangle + 2\nu\left\langle\frac{\partial u_j}{\partial x_k}\cdot\frac{\partial p}{\partial x_k}\right\rangle\right] = \frac{\partial}{\partial x_j}\left(\frac{\rho\nu_T}{\sigma_\varepsilon}\frac{\partial\varepsilon}{\partial x_j}\right) \quad (25)$$

$$-2\rho\nu\left\langle\frac{\partial u_i}{\partial x_k}\cdot\frac{\partial u_j}{\partial x_k}\cdot\frac{\partial u_i}{\partial x_j}\right\rangle - 2\rho\nu^2\left\langle\left(\frac{\partial^2 u_i}{\partial x_j\partial x_k}\right)^2\right\rangle = -C_{\varepsilon 1}\frac{\varepsilon}{k}\tau_{ij}\frac{\partial U_i}{\partial x_j} - \rho C_{\varepsilon 2}\frac{\varepsilon^2}{k} \quad (26)$$

$$\rho U_j\frac{\partial\varepsilon}{\partial x_j} = \frac{\partial}{\partial x_j}\left(\rho\frac{\nu_T}{\sigma_\varepsilon}\cdot\frac{\partial\varepsilon}{\partial x_j}\right) - \left[C_{\varepsilon 1}\tau_{ij}\frac{\partial U_i}{\partial x_j} + \rho C_{\varepsilon 2}\varepsilon\right]\frac{\varepsilon}{k} + \quad (28)$$
$$-C_{\varepsilon 1}\rho g\frac{\varepsilon}{k}\cdot\frac{\nu_T}{\sigma_T T_\infty}\cdot\frac{\partial T}{\partial z}$$

$$\rho\left[U_y\frac{\partial\varepsilon}{\partial y} + U_z\frac{\partial\varepsilon}{\partial z}\right] = \frac{\partial}{\partial y}\left(\rho\frac{\nu_T}{\sigma_\varepsilon}\cdot\frac{\partial\varepsilon}{\partial y}\right) + \frac{\partial}{\partial z}\left(\rho\frac{\nu_T}{\sigma_\varepsilon}\cdot\frac{\partial\varepsilon}{\partial z}\right) + \quad (29)$$
$$-\left[C_{\varepsilon 1}P_K + \rho C_{\varepsilon 2}\varepsilon\right]\frac{\varepsilon}{k} - C_{\varepsilon 1}\rho g\frac{\varepsilon}{k}\cdot\frac{\nu_T}{\sigma_T T_\infty}\cdot\frac{\partial T}{\partial z}$$

Equations 23, 24, 25, 26, 28, and 29.

equations and two relations presented above. The set of equations constitutes continuity equation (3), which in Cartesian coordinates assumes the form of

$$\frac{\partial}{\partial y}(\rho U_y) + \frac{\partial}{\partial z}(\rho U_z) = 0 \quad (30)$$

momentum Equations (10) and (11), the energy conservation Equation (15), the turbulent kinetic energy Equation (22) and the kinetic energy dissipation rate Equation (29). The two relations define the turbulent kinematic viscosity coefficient (6) and the equation of state of the perfect gas. The complex system of partial differential equations will be solved numerically with the aid of the computer program FLUENT [12] using the finite difference method.

The computation conditions

Now we present geometrical and physical conditions of the melt blowing process, which is the subject of the computations. The geometry of a dual slot die for blowing air is shown in ***Figure 1***. The polymer in the pneumatic melt spinning is extruded from a spinneret cylindrical orifice of 0.35 mm in diameter and blown in the z-direction by the symmetrical dual air jet. The polymer extrusion orifice is recessed by 0.3 mm from the spinning beam face. The width of the spinneret at the polymer outflow is D = 0.5 mm, which is also the distance between the air slots at the air outflow. The air is blown on both sides from the slots, which are inclined symmetrically at an angle of α = 28.25° to the z-axis. The lowest width of the air slots is at the outflow- b = 0.5 mm. The length of the air slots in the x-direction is of the order of one meter, and it is so large compared to the t with b of the slots that the air flow may be treated as two-dimensional in the plane (y, z).

Computations will be performed for the following initial values of the parameters of the air field at the outflow from the slots:

- initial air velocity: U_{j0} = 30, 50, 75, 100, 200 and 300 m/s,
- initial air temperature: T_{j0} = 573 K,
- initial air pressure: $P_{j0} = 1.015\times10^5$ N/m^2.

At the initial parameters: air density $\rho = 0.6172$ kg/m^3 and the dynamic viscosity coefficient $\mu = 2.97\times10^{-5}$ N·s/m^2, the kinematic viscosity coefficient is $\nu = \mu/\rho = 4.812\times10^{-5}$ m^2/s.

From the Reynolds number, $Re = U_{j0}b/\rho$, we can estimate the character of the air flow for chosen values of the initial air velocity. For U_{j0} = 30 m/s we have Re = 312, for U_{j0} = 75 m/s - Re = 780, and for U_{j0} = 300 m/s - Re = 3120. Reynolds numbers of 312 and 780 are not high, but according to the author [13], free jets with a Reynolds number between 300 and 800 are turbulent. For this reason we model the discussed air flow as turbulent. For higher Reynolds numbers the turbulent character of air flow is obvious.

Now we shall determine the air flow Mach number, $Ma = U_{j0}/a$, where the sound velocity $a = (\kappa R T_{j0})^{1/2}$, and R is the gas constant. For the air flow field, the ratio of the specific heats is $\kappa = C_p/C_v = 1.4$ and the sound velocity $a \cong 480$ m/s. For the air velocity U_{j0} = 30 m/s, the Mach number is rather small - Ma = 0.0625, but for U_{j0} = 100 m/s it is 0.208, and for U_{j0} = 300 m/s we get 0.625. Hence, the air in this process should be considered as compressible fluid.

The boundary conditions

The boundary conditions for the set of equations of the turbulent air flow field at the spinneret face, $z = 0$, $0 \le y \le D/2$, and at the slot die face, $z = 0.3$ mm, $y > D/2 + b\cos\alpha$, read

$$U_y = U_z = k = \varepsilon = 0, \quad \frac{\partial T}{\partial z} = 0, \ P = P_\infty \tag{30}$$

where P_∞ is the ambient atmospheric pressure.

At the slot outlet,

$$0 < z < 0.3 \text{ m}, \quad D/2 < y < D/2 + z\ ctg\ \alpha,$$

we get

$$U_y = U_{y0} = -U_{j0}\cos\alpha, \quad U_z = U_{z0} = U_{j0}\sin\alpha, \quad P = P_{j0} \tag{31}$$

$$T = T_{j0}, \quad k = 0.06\,(U_{y0}^2 + U_{z0}^2), \quad \varepsilon = 0.06\,(U_{y0}^3 + U_{z0}^3)/(b\cos\alpha) \tag{32}$$

At a large distance from the slot die- $z \to \infty$, the unknown quantities are constant

$$\frac{\partial U_z}{\partial z} = \frac{\partial T}{\partial z} = \frac{\partial k}{\partial z} = \frac{\partial \varepsilon}{\partial z} = 0, \quad U_y = 0, \ P = P_\infty \tag{33}$$

The flow is symmetrical with respect to the z-axis, hence the air conditions at the centerline of the flow in the (y, z) plane are as follows

$$\frac{\partial U_z}{\partial y} = \frac{\partial T}{\partial y} = \frac{\partial k}{\partial y} = \frac{\partial \varepsilon}{\partial y} = \frac{\partial P}{\partial y} = 0, \quad U_y = 0 \tag{34}$$

At a large distance from the centerline (z-axis), $y \to \infty$, we get

$$U_z = k = \varepsilon = 0, \quad T = T_\infty, \ \frac{\partial U_y}{\partial y} = 0, \ P = P_\infty \tag{35}$$

The constants of the k-ε model presented are as follows: $C_\mu = 0.09$, $C_{\varepsilon1} = 1.44$, $C_{\varepsilon2} = 1.92$, while the physical parameters of the air jet read:

- the specific heats at constant pressure: C_p = 1006.43 J/kg·K, and at constant volume: C_v = 718.88 J/kg·K,
- the heat conductivity coefficient: $\lambda = 0.0242$ W/m·K,
- the Prandtl number of turbulence: $\sigma_T = 0.85$, the Prandtl number of the turbulent kinetic energy: $\sigma_K = 1.00$, and the Prandtl number of the dissipation rate of the turbulent kinetic energy: $\sigma_\varepsilon = 1.30$.

Results of the computations and discussion

Computations are performed for the following six values of initial air jet velocities at the slot outlet: U_{j0} = 30, 50, 75, 100, 200 and 300 m/s. The flow field is limited by the slots within the range $0 \le z \le 0.3$ mm (***Figure 1*** see page 18), whereas below the spinning beam- $z > 0.3$ mm, the flow is unlimited.

Computations of the flow are performed for a limited range in all directions, so that it would be possible to make a net structure which allows for an efficient solution of the set of equations. However, the flow field considered in the computations is large enough with respect to the dimensions of the slots, and the results represent the dynamics of the air jet active in the pneumatic process. The approach allows to assume boundary conditions at chosen limits of the field, which gives a satisfactory approximation of the real conditions. Taking into account the experience of the other authors [6,7], we accept the following dimensions of the air flow field: we determine the filed limit at a distance y_{max} = 60 mm and y_{min} = −60 mm in the y-direction, in both directions from the z-axis, which is the centerline axis of symmetry. In the z-direction we accept the limit z_{max} = 200 mm. With these limits, the boundary conditions assumed above are valid.

In the computation technique the flow field is covered by a computation net with use of the FLUENT package [12]. The net grids are concentrated at the dual slot die, especially in the proximity of the slots, and they enlarge by increasing the distance from the die in the direction of the field boundaries. The number of grids in the entire field is about 100,000. The system of differential equations is solved using the iteration method with an iteration number of the order of 10,000.

Computations were performed for six initial air velocities chosen, and the results are presented in ***Figures 2 - 11*** (see page 22 and 23). In the Figures, we do not present the full field of velocity, temperature and pressure obtained in the computational domain. We limit the presentation of results to the distribution of the flow characteristics along the jet centerline which coincides with the z-axis, since this is also the axis of the pneumatic melt spinning process.

Distribution of the axial component of the air jet velocity along the z-axis, $V_a(z) = U_z(0, z)$, computed for the lower values of the initial air velocity - U_{j0} = 30, 50, 75 m/s and for higher values - U_{j0} = 100, 200, 300 m/s are presented in ***Figures 2*** and ***3***, respectively. Velocity plots are shown within a range shortened to 50 mm from the spinneret face to show details of the air jet that are important for pneumatic melt spinning taking place within a short distance from the spinneret. We see from the plots presented that in the vicinity of the dual slot die, where the spinneret is recessed from the spinning beam face by 0.3 mm (see ***Figure 1***), we have negative axial air velocity, which immediately inverts its direction and then rapidly increases with distance z. The axial air jet velocity reaches a maximum close to the die distance and then softly decreases with increasing z. Maximum axial jet velocity occurs at a distance of several millimeters from the spinneret face, and the distance increases with the rising initial air velocity U_{j0}. For

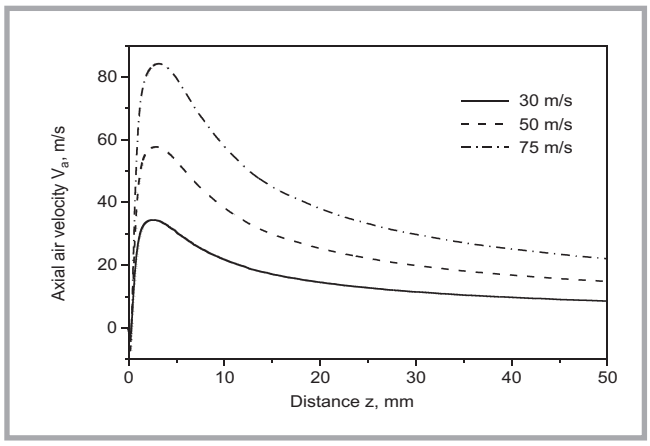

Figure 2. *Axial velocity profiles of the air jet along the centerline V_a vs. the distance from the spinneret z, computed for lower initial air velocities- U_{j0}=30, 50 and 75 m/s.*

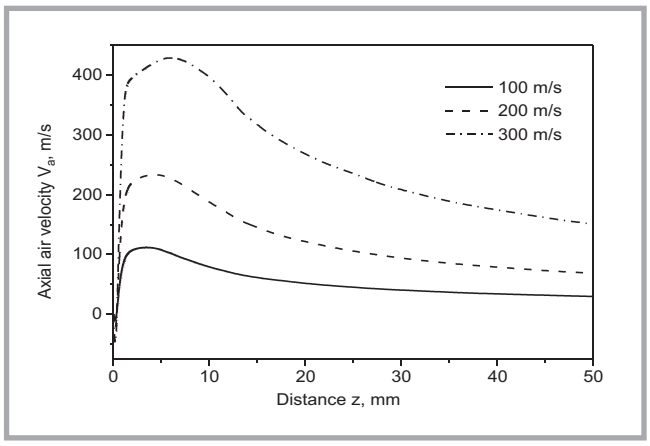

Figure 3. *Axial velocity profiles of the air jet along the centerline V_a vs. the distance from the spinneret z computed for higher initial air velocities- U_{j0}=100, 200 and 300 m/s.*

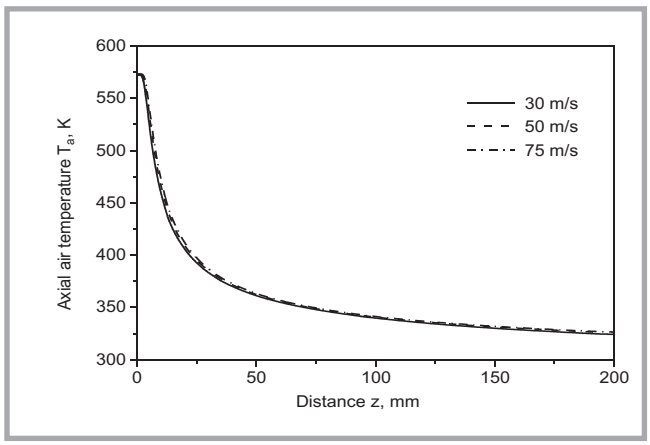

Figure 4. *Axial temperature profiles of the air jet along the centerline- T_a vs. the distance from the spinneret- z, computed for lower initial air velocities- U_{j0}=30, 50 and 75 m/s.*

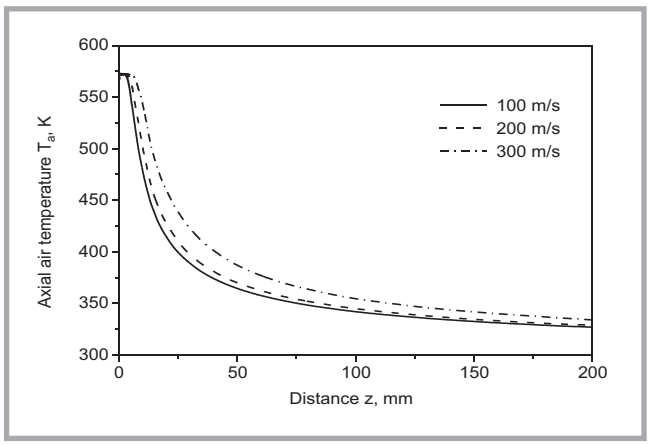

Figure 5*.Axial temperature profiles of the air jet along the centerline T_a vs. the distance from the spinneret z computed for higher initial air velocities- U_{j0}=100, 200 and 300 m/s.*

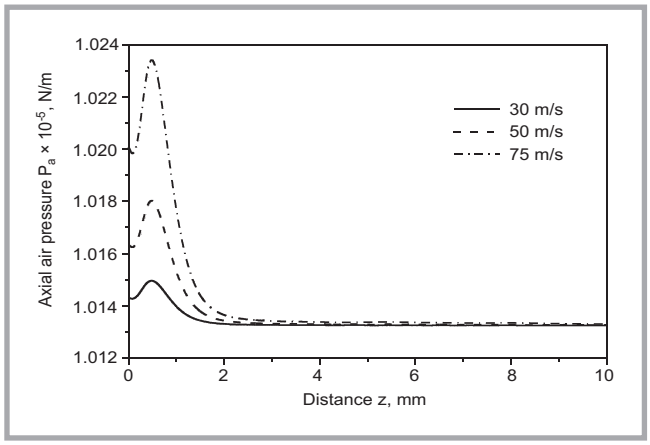

Figure 6. *Axial air pressure profiles along the centerline P_a vs. the distance from the spinneret z computed for lower initial air velocities, U_{j0}=30, 50 and 75 m/s.*

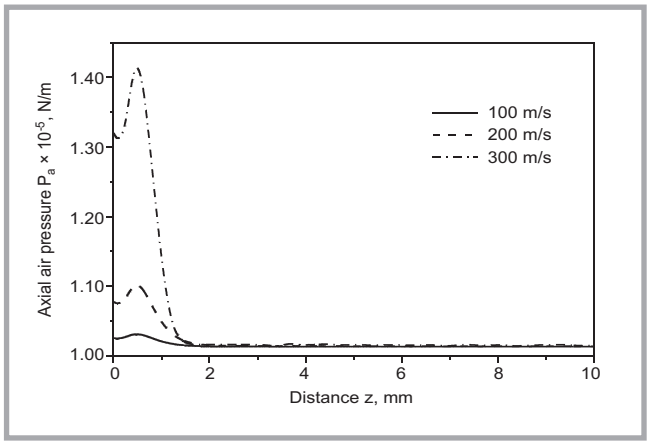

Figure 7. *Axial air pressure profiles along the centerline P_a, vs. the distance from the spinneret z computed for higher initial air velocities- U_{j0}=100, 200 and 300 m/s.*

the highest initial air velocity of 300 m/s, the maximum is predicted at a distance of 10 mm. The maximum values of the air velocity $U_{z,max}$ calculated are higher than the initial jet velocities U_{j0}. The air jets which flow symmetrically out of the dual slot die collide at the symmetry plane $y = 0$. Hence, the axial component of the air velocity at the centerline of the (y,z) plane increases above the initial air jet velocity. For lower initial jet velocities, the maximum value $U_{z,max}$ is above U_{j0} by about 15%, while for a high initial jet velocity of U_{j0} = 300 m/s, it attains a value of 430 m/s, about 40% higher. However, even the highest $U_{z,max}$ value obtained does not exceed the sound velocity, which is a = 480 m/s at the tem-

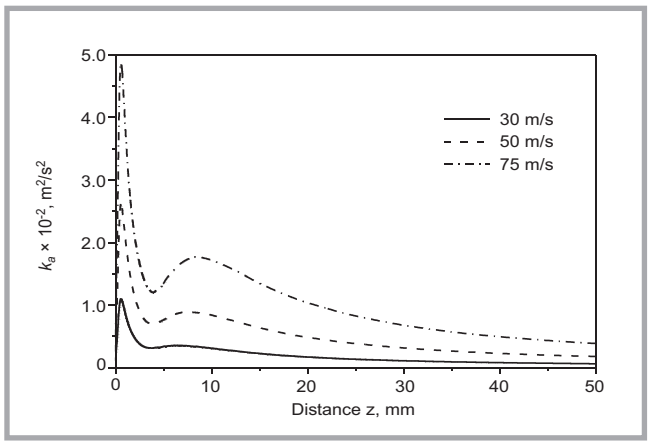

Figure 8. *Axial distribution of the turbulent kinetic energy along the centerline k_a vs. the distance from the spinneret z computed for lower initial air velocities- U_{j0}=30, 50 and 75 m/s.*

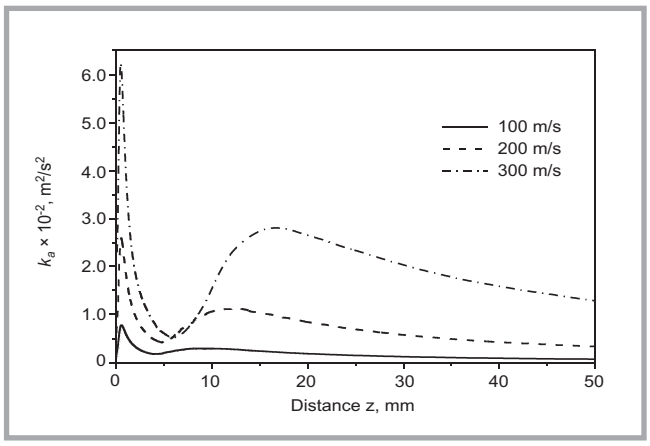

Figure 9. *Axial distribution of the turbulent kinetic energy along the centerline k_a vs. the distance from the spinneret z computed for higher initial air velocities, U_{j0}=100, 200 and 300 m/s.*

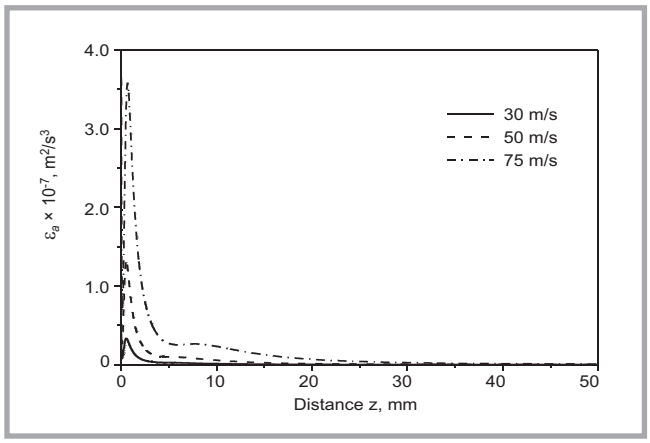

Figure 10. *Axial distribution of the kinetic energy dissipation rate along the centerline ε_a vs. the distance from the spinneret z computed for lower initial air velocities- U_{j0}=30, 50 and 75 m/s.*

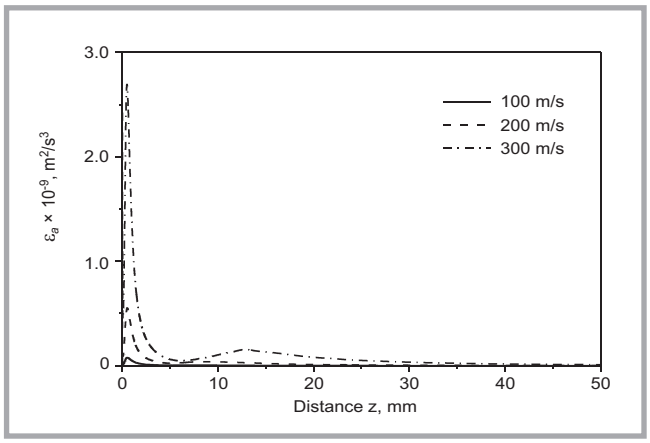

Figure 11. *Axial distribution of the kinetic energy dissipation rate along the centerline ε_a vs. the distance from the spinneret z computed for higher initial air velocities- U_{j0}=100, 200 and 300 m/s.*

perature of 573 K, where the assumed air flow remains sub-critical. The plots shown in ***Figures 2*** and ***3*** are qualitatively similar to the velocity diagrams obtained by other authors [7, 11].

Figures 4 and ***5*** present axial distributions of the air temperature along the jet centerline- $T_a(z) = T(0, z)$, and ***Figures 6*** and ***7*** illustrate the air pressure distributions- $P_a(z) = P(0, z)$ computed for three lower and three higher values of initial air velocities. The pressure distribution is presented in the distance range $0 \le z \le 10$ mm, shortened with respect to the full computational range, for the purpose of illustration, because only in this range does the pressure distribution differ from that of the the atmospheric in a noticeable way.

The kinetic energy k_a and dissipation rate ε_a evidently grow with the air velocity. It is seen in ***Figures 8*** and ***9*** that the kinetic energy close to the spinneret face is about one order higher for a velocity of 75 m/s than for 30 m/s and for the velocity 300 m/s than for 100 m/s. The same may be observed for the dissipation rate in ***Figures 10*** and ***11***. It is the reason why the axial temperature T_a grows with the air velocity, which is particularly evident in ***Figure 5***.

Acknowledgment

This paper resulted from research supported by Research Grant Nr 3 T08E 08628 from the Polish State Committee for Scientific Research, Poland.

References

1. *U.S. Patent 3,849,241 (1974).*
2. *U.S. Patent 3,825,380 (1974).*
3. *L. Gerking, Chemical Fibers International, 52, 2002, 424.*
4. *R.R. Bresee, W.C. Ko, International Nonwovens J., 2003, Summer, 21.*
5. *R.R. Bresee, International Nonwovens J., 2004, Spring, 36.*
6. *T. Chen, X. Wang, X. Huang, Textile Research J., 74, 2004, 1018.*
7. *H. M. Krutka, R. I. Shambaugh, D. V. Papavassiliou, Ind. Eng. Chem. Res., 42, 2003, 5541.*
8. *J. W. Elsner, Turbulencja Przepływów, PWN, Warszawa, 1987, pp. 69-79, 95-100.*
9. *B. Mohammadi, O. Pironneau, Analysis of the K – Epsilon Turbulence Model, John Wiley & Sons, Chichester, MASSON S.A. Paris 1994, p.51-62.*
10. *D.C. Wilcox, Turbulence Modeling for CFD (Computational Fluid Dynamics), DCW Industries, Inc., La Canada, California, 1984, p.176-183.*
11. *S.B. Pope, Turbulent Flows, Cambridge University Press, Cambridge 2000, pp. 83-95, 95-100.*
12. *FLUENT Inc. Fluent 6.1 User's Guide, Lebanon, NH, 2003.*
13. *A. Boguslawski, Technical University of Czestochowa, 2006 (private communication).*
14. *H.M. Krutka, R.I. Shambaugh, D.V. Papavassiliou, International Nonwovens J., 2005, Spring, 2.*

Received 08.11.2007 Reviewed 13.12.2007